





# Nucleosynthesis signatures of neutrino-driven winds from proto-neutron stars: a perspective from chemical evolution models

Fiorenzo Vincenzo <sup>1</sup>★, Todd A. Thompson <sup>1</sup>, David H. Weinberg,<sup>1,2</sup> Emily J. Griffith <sup>1</sup>, James W. Johnson <sup>1</sup> and Jennifer A. Johnson<sup>1</sup>

<sup>1</sup>*Department of Astronomy & Center for Cosmology and AstroParticle Physics, The Ohio State University, Columbus, OH 43210, USA*

<sup>2</sup>*Institute for Advanced Study, Princeton, NJ 08540, USA*

Accepted 2021 September 27. Received 2021 September 6; in original form 2021 February 9

## ABSTRACT

We test the hypothesis that the observed first-peak (Sr, Y, Zr) and second-peak (Ba) s-process elemental abundances in low-metallicity Milky Way stars, and the abundances of the elements Mo and Ru, can be explained by a pervasive r-process contribution originating in neutrino-driven winds from highly magnetic and rapidly rotating proto-neutron stars (proto-NSs). We construct chemical evolution models that incorporate recent calculations of proto-NS yields in addition to contributions from asymptotic giant branch stars, Type Ia supernovae, and two alternative sets of yields for massive star winds and core-collapse supernovae. For non-rotating massive star yields from either set, models without proto-NS winds underpredict the observed s-process peak abundances by 0.3–1 dex at low metallicity, and they severely underpredict Mo and Ru at all metallicities. Models incorporating wind yields from proto-NSs with spin periods  $P \sim 2\text{--}5$  ms fit the observed trends for all these elements well. Alternatively, models omitting proto-NS winds but adopting yields of rapidly rotating massive stars, with  $v_{\text{rot}}$  between 150 and 300 km s<sup>−1</sup>, can explain the observed abundance levels reasonably well for  $[\text{Fe}/\text{H}] < -2$ . These models overpredict  $[\text{Sr}/\text{Fe}]$  and  $[\text{Mo}/\text{Fe}]$  at higher metallicities, but with a tuned dependence of  $v_{\text{rot}}$  on stellar metallicity they might achieve an acceptable fit at all  $[\text{Fe}/\text{H}]$ . If many proto-NSs are born with strong magnetic fields and short spin periods, then their neutrino-driven winds provide a natural source for Sr, Y, Zr, Mo, Ru, and Ba in low-metallicity stellar populations. Conversely, spherical winds from unmagnetized proto-NSs overproduce the observed Sr, Y, and Zr abundances by a large factor.

**Key words:** stars: abundances – stars: magnetars – Galaxy: abundances.

## 1 INTRODUCTION

Isotopes with nucleon number larger than that of iron-peak elements ( $\mathcal{A} \approx 56$ ) are prevented by an increasingly large Coulomb barrier from being synthesized by any charged-particle-induced thermonuclear reaction in stellar interiors. The existence of the vast majority of the trans-iron elements is explained by a series of neutron-capture processes followed by  $\beta$ -decays, starting from seed nuclei of iron-peak elements (Burbidge et al. 1957; Cameron 1957). Neutron-capture nucleosynthesis can operate by means of two processes, depending on whether the rate of neutron capture is slow (s-process) or rapid (r-process) with respect to the rate of  $\beta$ -decay. Nearly all trans-iron elements are produced by a mixture of s- and r-process events, except for a number of stable s-only nuclei that are shielded from any r-process contribution by the presence of a stable, neutron-rich r-only nucleus with equal  $\mathcal{A}$ .

In the classical picture, the s-process proceeds along the so-called valley of  $\beta$ -stability, giving rise to three distinctive peaks in the solar abundance template, which correspond to the magic neutron numbers  $\mathcal{N}_n = 50$  (e.g. <sup>88</sup>Sr, <sup>89</sup>Y, <sup>90</sup>Zr),  $\mathcal{N}_n = 82$  (e.g. <sup>138</sup>Ba), and  $\mathcal{N}_n = 126$  (e.g. <sup>208</sup>Pb). Such peaks in the solar abundance pattern are due to the fact that the stable heavy-element isotopes with a magic

neutron number have a neutron-capture cross-section that is much lower than that of the other isotopes of the  $\beta$ -stability valley, creating a bottleneck in the s-process path.

The main site of the s-process nucleosynthesis in astrophysical environments is found in the late evolutionary stages of low- and intermediate-mass (LIM) stars, during the asymptotic giant branch (AGB) phase (e.g. Ulrich 1973). The main source of free neutrons in AGB stars is provided by the reaction <sup>13</sup>C( $\alpha, n$ )<sup>16</sup>O (Iben & Renzini 1982; Hollowell & Iben 1989), which is active at energies  $E \approx 8$  keV. The formation of the so-called <sup>13</sup>C-pocket in the He intershell during the interpulse period of AGB stars represents the key physical mechanism responsible for the s-process nucleosynthesis in LIM stars (Iben & Renzini 1982; Hollowell & Iben 1989; Straniero et al. 1995; Gallino et al. 1998; Straniero, Cristallo & Gallino 2009). The continuous recurrence of the third dredge-up and interpulse periods makes s-process nucleosynthesis in AGB stars very effective for a relatively extended period of time, producing remarkable effects in the chemical abundance distribution observed in the stars of our Galaxy (see e.g. Busso et al. 2001; Karakas & Lattanzio 2007; Cristallo et al. 2009; Karakas & Lugaro 2016).

s-process nucleosynthesis can also take place during the evolutionary stage of core He burning of massive stars, which – before exploding as core-collapse supernovae (SNe) – can pollute the interstellar medium (ISM) of our Galaxy through radiatively driven stellar winds, enriched with He, C, N, O, and traces of s-process elements.

\* E-mail: vincenzo.3@osu.edu

In particular, massive stars provide a prompt s-process contribution to the chemical evolution of our Galaxy at low metallicities, before low-mass stars reach the AGB phase and enrich the ISM with their nucleosynthetic products. An interesting study is that of Cescutti et al. (2013), who proposed that a prompt s-process contribution from rapidly rotating massive stars (Frischknecht, Hirschi & Thielemann 2012) – predicted to be more abundant at low metallicities, where stars are more compact and hence rotate faster – can help explain the shape of the scatter in  $[\text{Sr}/\text{Ba}]$  in metal-poor halo stars (see also the review of Frebel 2010).

The r-process works by rapidly piling up neutrons in an increasingly heavy nucleus. As the neutron capture proceeds, the nucleon binding energy becomes increasingly low, until an equilibrium is reached between the photodisintegration and the neutron capture, which temporarily freezes out the neutron number. The  $\beta$ -decay of the neutron-rich nucleus then breaks the deadlock, allowing the r-process to resume. It then proceeds rapidly until a new equilibrium is reached again (see e.g. the classical books of Clayton 1983; Rolfs & Rodney 1988).

The r-process is the main physical mechanism behind the nucleosynthesis of the neutron-rich heavy elements observed in Milky Way (MW) stars at all metallicities, but it also provides a non-negligible contribution to the majority of neutron-capture elements that are observed in metal-poor stars. The signature of r-process events is very pervasive, and it is observed at all metallicities in the stars of our Galaxy.

The astrophysical environments of r-process events in the cosmos usually involve explosive physical conditions, because very high neutron densities are required. The neutron-rich isotopes produced along the r-process path have a very short half-life, causing the neutron-rich nuclei to  $\beta$ -decay over time-scales of the order of milliseconds, if they did not undergo further rapid neutron capture. Examples of r-process sites that have been proposed and investigated by theoretical studies include (i) neutrino-driven winds from proto-neutron stars (NSs; Takahashi, Witt & Janka 1994; Woosley et al. 1994; Qian & Woosley 1996; Hoffman, Woosley & Qian 1997; Otsuki et al. 2000; Thompson, Burrows & Meyer 2001; Wanajo et al. 2009; Hansen et al. 2013; Wanajo 2013); (ii) neutrino-driven winds from highly magnetic and potentially rapidly rotating proto-magnetars (Thompson 2003; Thompson, Chang & Quataert 2004; Metzger, Thompson & Quataert 2007, 2008; Vlasov, Metzger & Thompson 2014; Vlasov et al. 2017; Thompson & ud-Doula 2018); (iii) neutrino-driven winds around the accretion disc of a black hole (Pruet, Thompson & Hoffman 2004; Metzger et al. 2008; Wanajo & Janka 2012; Siegel, Barnes & Metzger 2019); (iv) electron-capture SNe (see e.g. Wanajo et al. 2009; Cescutti et al. 2013; Kobayashi, Karakas & Lugaro 2020); (v) magneto-rotationally driven SNe (Burrows et al. 2007; Winteler et al. 2012; Cescutti & Chiappini 2014; Mösta et al. 2014, 2015, 2018; Nishimura, Takiwaki & Thielemann 2015; Nishimura et al. 2017; Halevi & Mösta 2018; Reichert et al. 2021); and (vi) neutron-star mergers (Lattimer et al. 1977; Freiburghaus, Rosswog & Thielemann 1999; Argast et al. 2004; Goriely, Bauswein & Janka 2011; Rosswog 2013; Matteucci et al. 2014; Cescutti et al. 2015; Vincenzo et al. 2015; Kobayashi et al. 2020). Since it is likely that all these mechanisms have contributed to r-process nucleosynthesis at some level, the theoretical studies have focused on exploring the frequency of each event and the predicted template of the corresponding r-process ejecta.

Due to the large uncertainties in the r-process nucleosynthesis calculations, the working strategy of the first MW chemical evolution models was to assume empirical yields for the r-process, which were tuned to reproduce the abundances of light and heavy neutron-

capture elements at low metallicity. After doing this, it was possible to discuss the conditions for the different r-process sites to produce enough material to explain the neutron-capture elemental abundances and their dispersion in metal-poor stars (e.g. Travaglio et al. 2004; Cescutti et al. 2006; Cescutti 2008). Another strategy was employed by Prantzos et al. (2018), who emphasize the rotating massive star contribution and fit the metallicity dependence of stellar rotation empirically by reproducing observed abundance trends (see also Prantzos et al. 2020). Kobayashi et al. (2020) recently explored the impact of a variety of different scenarios to the observed abundances of neutron-capture elements.

In this work, we explore the hypothesis that neutrino-driven winds from proto-NSs can explain the abundances of the first peak (Sr, Y, Zr) and second peak (Ba) of the s-process elemental abundance distribution. We test this hypothesis by assuming that massive stars enrich the ISM at their death through (i) radiative-driven mass-loss; (ii) core-collapse SNe; and – after the explosion – (iii) neutrino-driven winds from the proto-NS that may have been left after the explosion. To test this hypothesis, we also look at the abundances of Mo and Ru, which can be synthesized in p-rich outflows of proto-NSs (Hoffman et al. 1996; Fröhlich et al. 2006; Pruet et al. 2006). Throughout this paper, when we consider proto-NS winds we mean both purely neutrino-driven proto-NS winds and proto-magnetar models with strong magnetic fields and potentially rapid rotation as described in Vlasov et al. (2017). We emphasize the latter scenario, which achieves good agreement with observations, while also showing that existing yield predictions for the winds from unmagnetized, non-rotating proto-NSs overproduce some observed abundances by a large factor (Hoffman et al. 1996, 1997). We note that other mechanisms mentioned above (e.g. NS–NS mergers, accretion discs, and magneto-rotational SNe) may all play additional roles, which would require models for their frequencies and relative yields. Recent studies indicate that  $\sim 40$  per cent of NS births produce magnetar-strength fields (Beniamini et al. 2019). Moreover, recent work by Sukhbold & Thompson (2017) argues that normal Type IIP SNe may arise from magnetars with few ms spin period. Nevertheless, while the spin distribution of NSs with magnetar-strength fields is highly uncertain, the observed spin distribution of normal pulsars indicates that their NSs are born rotating slowly; a typical average value of the initial spin period is  $\langle P \rangle = 300$  ms, with  $\sigma_P = 150$  ms (table 6 of Faucher-Giguère & Kaspi 2006).

Our paper is organized as follows. In Section 2, we describe our chemical evolution model. In Section 3, we present our results. Finally, in Section 4, we draw our conclusions.

## 2 THE MODEL

We develop a chemical evolution model for the abundances in the ISM of our Galaxy, which makes the following assumptions for the various stellar and SN chemical enrichment sources.

(i) For AGB stars, we assume the stellar nucleosynthesis yields as computed by Straniero, Gallino & Cristallo (2006), Cristallo et al. (2007, 2009, 2011, 2015a, b, 2016), Piersanti, Cristallo & Straniero (2013), and Straniero, Cristallo & Piersanti (2014), which are publicly available online at the FRUITY database website.<sup>1</sup> Our assumed set of stellar yields for AGB stars includes the following metallicities  $Z = 0.00002, 0.00005, 0.0001, 0.0003, 0.001, 0.002, 0.003, 0.006, 0.008, 0.01, 0.014, 0.02$ , with stellar masses in the range  $1.3 < M < 6.0 M_{\odot}$ .

<sup>1</sup><http://fruity.oa-teramo.inaf.it>

(ii) We consider two alternatives for massive star yields. Our reference model assumes the stellar nucleosynthesis yields as computed by Sukhbold et al. (2016) for non-rotating stars with masses in the range  $9 \leq M < 120 M_{\odot}$  at solar metallicity, which account for black hole formation and ‘failed’ SNe (see e.g. Ugliano et al. 2012; Pejcha & Thompson 2015; Ertl et al. 2016; Sukhbold & Adams 2020 for simulations and models, and Smartt 2009; Gerke, Kochanek & Stanek 2015; Adams et al. 2017; Basinger et al. 2021 for an observational perspective). Specifically, we use the yields provided for the Z9.6 model below  $12 M_{\odot}$  and the W18 model at higher masses. Sukhbold et al. (2016) compute yields at solar metallicity, which we apply at all metallicities. With the W18 central engine, most stars between  $22\text{--}25 M_{\odot}$  and above  $28 M_{\odot}$  form black holes without explosion, but they still produce enrichment through stellar winds. Note that the nucleosynthesis calculations of Sukhbold et al. (2016) do not account for neutrino interactions during the collapse and explosion, which can affect the evolution of  $Y_e$  and hence the nucleosynthesis of the innermost ejecta, modifying the abundances of the immediate post-shock ejecta during the explosion (see Fröhlich et al. 2005, 2006; Pruet et al. 2005; Curtis et al. 2019; Ebinger et al. 2020), generating some p-rich elements. We do not include a complete description of the innermost ejecta, but we do adopt abundances for the p-rich elements Mo and Ru, which can be produced in p-rich proto-NS winds (Pruet et al. 2006). In this way, our chemical evolution models combine the nucleosynthesis calculations of Sukhbold et al. (2016) for core-collapse SNe with the models of Pruet et al. (2006) for proto-NS winds, which include the potential for p-rich wind material.

Our alternative massive star yields use the calculations of Limongi & Chieffi (2018, set R) with stellar rotation velocity  $v_{\text{rot}} = 150 \text{ km s}^{-1}$  and the following grid of iron abundances:  $[\text{Fe}/\text{H}] = -3, -2, -1, 0, 2$ . We note that Limongi & Chieffi (2018) also account for failed SNe, by assuming a sharp transition at  $M > 25 M_{\odot}$ . Above this threshold mass, the chemical enrichment is provided only by the stellar winds.

(iii) The average yields of Sr, Y, and Zr from neutrino-driven winds from proto-NSs are taken from the models of Vlasov et al. (2017) with rotation periods  $P = 2, 3, 5,$  and  $10$  ms. For Ba, our reference model assumes an average yield  $M_{\text{Ba},r} = 5 \times 10^{-7} M_{\odot}$ , which is of the order of magnitude predicted in the winds of the most massive proto-NSs by Wanajo (2013). Note that Vlasov et al. (2017) find very little Ba production in all of their models. However, they did not systematically consider higher mass proto-NSs and they did not include the effects of general relativity (GR), both of which enhance heavy-element production (Cardall & Fuller 1997), and were considered by Wanajo (2013). Conversely, Wanajo (2013) did not consider the effects of a strong magnetic field and rapid rotation on the nucleosynthesis, which Vlasov et al. (2017) find have important consequences for production of elements  $Z < 55$ . For these reasons, we take the Sr, Y, Zr abundances from Vlasov et al. (2017) and take the Ba abundances from Wanajo (2013) under the assumption that Vlasov et al. (2017)-like models including GR and a range of higher proto-NS masses would yield results for Ba more like the Wanajo (2013) yields. The calculations of Wanajo (2013) adopt a fixed  $Y_e = 0.4$  that is optimistic from the point of view of  $r$ -process nucleosynthesis. The value  $Y_e = 0.4$  is near, but below, the most neutron-rich value of  $Y_e$  obtained in the proto-NS cooling calculations used in Vlasov et al. (2017). It is not clear whether such low values of  $Y_e$  can be attained generically for all proto-NS masses and rotation rates.

Conversely, the models of Vlasov et al. (2017) adopt the full proto-NS cooling calculation of Roberts, Woosley & Hoffman (2010) for a non-rotating  $1.4 M_{\odot}$  proto-NS, which represents an up-to-date and modern calculation predicting low  $Y_e < 0.5$  in the wind cooling epoch. However, the predicted  $Y_e$  never decreases below 0.44 and eventually becomes proton-rich after approximately 6 s of cooling. It is unclear how the proto-NS cooling calculations would generalize to the range of masses considered by Wanajo (2013) or the rapid rotation and strong magnetic effects employed by Vlasov et al. (2017), since one expects the details of the cooling process, and the resulting wind  $Y_e$  to depend on both mass and rotation. Because Wanajo (2013) uses a fixed, optimistic value of  $Y_e = 0.4$  for a range of masses, we use it as a measure of the uncertainty in the Ba production. The details of both the wind and explosion nucleosynthesis can be further modified by multidimensional effects such as continued accretion during the explosion as the wind emerges; in this regard, Bollig et al. (2021) suggest that the wind develops only in the lowest mass progenitor cases due to a long-term accretion flow, which hinders the neutrino-driven wind. All these issues point to the urgent need for a next generation of magnetic and rapidly rotating proto-NS wind models including GR, a range of proto-NS masses, and dynamical magnetospheres (see Thompson & ud-Doula 2018).

Since the wind calculations of Vlasov et al. (2017) do not address the physics of the  $\nu p$ -process giving rise to high- $Y_e$  early ejecta, we adopt the models of Pruet et al. (2006) for the chemical elements Mo and Ru. In particular, the production factors for the most abundant isotopes of Mo and Ru,  $P_{\text{Mo,Ru}}$ , are in the range 10–30, according to the predictions of the models of Pruet et al. (2006), with the average yield of  $i = \text{Mo, Ru}$  being defined as

$$M_{i,\text{pnw}}(m) = P_i \times X_{\odot,i} \times M_{\text{tot-ej,SN}}(m), \quad (1)$$

where  $X_{\odot,i}$  is the solar abundance by mass of  $i = \text{Mo, Ru}$  (Asplund et al. 2009) and  $M_{\text{tot-ej,SN}}(m)$  is the total ejected mass in the core-collapse SN explosion of a massive star with initial mass  $m$ .

(iv) For Type Ia SNe, we assume the empirically motivated delay-time distribution function (DTD; Maoz & Mannucci 2012):

$$\text{DTD}_{\text{Ia}}(t) = A_{\text{Ia}} t^{-1.1}, \quad (2)$$

where  $A_{\text{Ia}}$  is chosen in order to have two Type Ia SNe over 13.8 Gyr per  $10^3 M_{\odot}$  of stellar mass formed (Bell et al. 2003; Maoz, Mannucci & Nelemans 2014; Vincenzo, Matteucci & Spitoni 2017). In this work, we assume a minimum delay-time  $\tau_{\text{min,Ia}} = 150$  Myr. The stellar yields of Type Ia SNe are from Iwamoto et al. (1999).

*The star formation rate* – We assume that the star formation rate (SFR) follows a linear Kennicutt law, namely  $\text{SFR}(t) = \text{SFE} \times M_{\text{gas}}(t)$ , where SFE represents the star formation efficiency and  $M_{\text{gas}}(t)$  is the total gas mass in the Galaxy.

*The accretion rate* – The simulated galaxy is assumed to form from the accretion of primordial gas from the circumgalactic environment. The gas infall rate obeys the following law:  $\mathcal{I}(t) = A_{\mathcal{I}} \times e^{-t/\tau_{\text{inf}}}$ , where  $A_{\mathcal{I}}$  is a normalization constant that determines the total amount of gas accreted over the Hubble time, defining the so-called infall-mass,  $M_{\text{inf}}$ , of the models.

*The outflow rate* – The model can account for the effect of galactic outflows, which carry gas and metals out of the galaxy potential well. The galactic winds are assumed to proceed with a rate proportional to the SFR, namely  $\mathcal{O}(t) = \omega \text{SFR}(t)$ , where  $\omega$  is the so-called mass-loading factor. We note in advance that our reference chemical evolution model – for simplicity – does not assume outflow activity ( $\omega = 0$ ).

<sup>2</sup>These stellar yields are publicly available at the following website: <http://orfeo.iaps.inaf.it>.

*The chemical-enrichment rate* – The chemical enrichment from winds of AGB stars and massive stars, core-collapse SNe, Type Ia SNe, and neutrino-driven winds from proto-NSs is included in our chemical evolution model according to the following equation:

$$\mathcal{R}_i(t) = \int_{m_{\text{TO}}(t)}^{m_{\text{cutoff}}} dm \text{ IMF}(m) \text{ SFR}(t - \tau_m) p_i(m, Z(t - \tau_m)) + p_{i,\text{Ia}} \int_{\tau_{\text{min,Ia}}}^t d\tau \text{ DTD}_{\text{Ia}}(\tau) \text{ SFR}(t - \tau), \quad (3)$$

which describes the chemical-enrichment rate of the  $i$ -th chemical element at the time  $t$  from all the assumed dying nucleosynthetic sources. In the reference model, we assume the initial mass function (IMF) of Kroupa, Tout & Gilmore (1993) and the stellar lifetimes,  $\tau_m$ , of Kobayashi (2004). Note that the Kroupa et al. (1993) IMF is quite different from the one usually referred to as a ‘Kroupa IMF’ (Kroupa 2001). It has a high-mass slope of  $-2.7$  rather than  $-2.3$ , and it therefore predicts lower IMF-averaged yields from massive stars for a given SFR.

The quantity  $m_{\text{TO}}(t)$  in equation (3) represents the turn-off mass, which is derived from the assumed inverse stellar lifetimes of Kobayashi (2004); the quantity  $m_{\text{cutoff}} = 100 M_{\odot}$  represents the maximum stellar mass, which is assumed to form in the star formation events; the quantity  $p_i(m, Z)$  represents the stellar nucleosynthetic yields of the  $i$ -th chemical element from all stars with mass  $m$  and metallicity  $Z$ ; finally,  $p_{i,\text{Ia}}$  is the average nucleosynthesis yield from Type Ia SNe. Note that  $p_i(m, Z)$  includes the nucleosynthesis yields from stellar winds of AGB stars and massive stars, core-collapse SNe, and neutrino-driven winds from proto-NSs. We assume that proto-NS winds arise for stars with progenitor masses  $8 \leq m < 20 M_{\odot}$  and that more massive progenitors produce black hole remnants with no proto-NS winds.

*The chemical evolution equations* – Using all quantities defined above, our model solves the following differential equation for the evolution of the gas mass in the form of the  $i$ -th chemical element in the ISM of the galaxy as a function of time:

$$\frac{dM_{g,i}(t)}{dt} = -X_i(t) \text{ SFR}(t) + \mathcal{R}_i(t) + \mathcal{I}(t) - \mathcal{O}(t), \quad (4)$$

where  $X_i(t) = M_{g,i}(t)/M_{\text{gas}}(t)$  is the ISM abundance by mass of the  $i$ -th chemical element at the time  $t$ . In our reference chemical evolution model, we assume  $\text{SFE} = 2 \text{ Gyr}^{-1}$ ,  $\tau_{\text{inf}} = 5 \text{ Gyr}$ ,  $\omega = 0$ ,  $\log(M_{\text{inf}}/M_{\odot}) = 11.5$ , which are tuned to reproduce the observed chemical abundance patterns of  $[X/\text{Fe}]$ – $[\text{Fe}/\text{H}]$ , where  $X = \text{O}, \text{Sr}, \text{Y}, \text{Zr}, \text{Ba}, \text{Mo},$  and  $\text{Ru}$ , at the solar neighbourhood. These values are consistent with previous works (e.g. Minchev, Chiappini & Martig 2013; Nidever et al. 2014; Spitoni et al. 2015; Vincenzo et al. 2017; Magrini et al. 2018). In contrast to the models of Andrews et al. (2017) and Weinberg, Andrews & Freudenberg (2017), we are able to obtain solar metallicities with  $\omega = 0$  because the steeper IMF and reduction of massive star yields by black hole formation lowers the IMF-averaged yields by a substantial factor. We run the model for a time interval of 10 Gyr.

### 3 RESULTS

The predictions of our reference chemical evolution model for the first peak  $s$ -process elemental abundance ratios are shown in Fig. 1. For  $[\text{Y}/\text{Fe}]$ , the observational data are from the second data release of the GALactic Archaeology with HERMES (GALAH) spectroscopic survey (2D histogram with the grey colour-coding; Buder et al. 2018), considering only dwarf stars with surface gravity  $\log(g) > 3.5$  and signal-to-noise ratio (SNR)  $> 20$ . To understand the

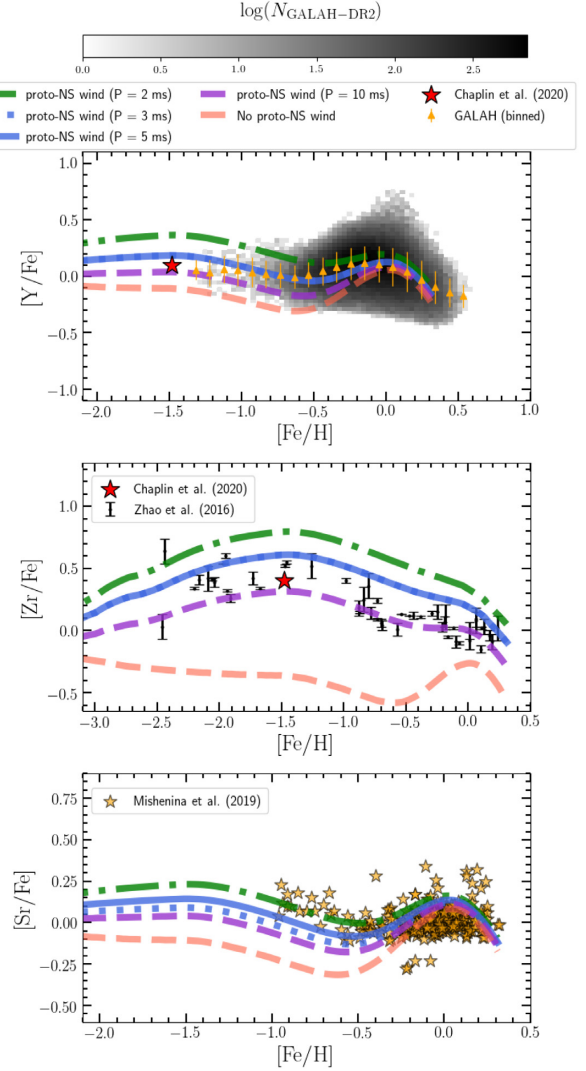


**Figure 1.** The predictions of chemical evolution models including a contribution to Sr, Y, and Zr from neutrino-driven winds of proto-NSs with different rotation periods (Vlasov et al. 2017) (green dash-dotted line:  $P = 2$  ms; blue dotted line:  $P = 3$  ms; blue solid line:  $P = 5$  ms; magenta solid line:  $P = 10$  ms). These models are compared with a model that does not assume proto-NS winds (red dashed curve), but only chemical enrichment from stellar winds of AGB stars (Cristallo et al. 2016) and massive stars (Sukhbold et al. 2016), and core-collapse SNe (Sukhbold et al. 2016). The observational data are from Zhao et al. (2016, black error bars), Mishenina et al. (2019, orange star symbols), and Chaplin et al. (2020, red star symbol). For Y, we also show the observational data from GALAH-DR2 (Buder et al. 2018), which are represented by the grey colour-code 2D histogram, as well as by the average binned data (yellow triangles with error bars), by selecting only dwarf stars with  $\log(g) > 3.5$  and signal-to-noise ratio (SNR)  $> 20$ . Model curves (not shown) that adopt the predicted yields of spherical winds from unmagnetized proto-NSs would be mostly off the top of these plots, exceeding the observed abundance ratios by 1–1.5 dex at all metallicities.

average trend of the data, we also show the mean  $[\text{Y}/\text{Fe}]$  from GALAH with the corresponding  $\pm 1\sigma$  dispersion as a function of  $[\text{Fe}/\text{H}]$  (yellow triangles with error bars). Finally, we show the  $[\text{Y}/\text{Fe}]$  ratio as measured by Chaplin et al. (2020) in a bright star belonging to the inner MW halo ( $\nu$  Indi) (red star symbol), for which they measured an asteroseismic age of  $\approx 11$  Gyr from the analysis of the *TESS* oscillation spectrum of the star. For  $[\text{Zr}/\text{Fe}]$ , the

observational data are from Chaplin et al. (2020, red star symbol) and Zhao et al. (2016, black data with error bars) for a sample of stars in the solar neighbourhood. For  $[\text{Sr}/\text{Fe}]$ , we show the abundance measurements of Mishenina et al. (2019, yellow star symbols). All observational data shown in Fig. 1 are measured by accounting for non-local thermodynamic equilibrium (NLTE) effects in the abundance analysis.

When accounting only for the chemical enrichment from core-collapse SNe, Type Ia SNe, and the stellar winds of AGB stars and non-rotating massive stars (pink dashed curve in Fig. 1), we cannot reproduce the observed abundance ratios of  $[\text{X}/\text{Fe}]$  of the first-peak s-process elements ( $X = \text{Sr}, \text{Y}, \text{Zr}$ ). In particular, our chemical evolution model consistently underpredicts the abundance ratios at metallicities below  $[\text{Fe}/\text{H}] \approx -0.5$ . Including the additional r-process contribution from neutrino-driven winds of proto-NSs with rotation periods in the range  $2 \leq P \leq 5$  ms, significantly improves the agreement with the data. For  $P = 10$  ms, the model underpredicts the observed  $[\text{Sr}/\text{Fe}]$  ratios at  $[\text{Fe}/\text{H}] \approx -1$ , though agreement with  $[\text{Y}/\text{Fe}]$  and  $[\text{Zr}/\text{Fe}]$  is acceptable. For  $P = 10$  ms, the proto-NS is effectively ‘non-rotating’ in the sense that the predicted yields would not decrease much for still longer periods.

Although we do not show them in Fig. 1, we have also computed models using the yields of the ‘spherical’ calculations of Vlasov et al. (2017) for non-rotating, unmagnetized proto-NS. These models overpredict the observed  $[\text{Y}/\text{Fe}]$ ,  $[\text{Zr}/\text{Fe}]$ , and  $[\text{Sr}/\text{Fe}]$  ratios by 1–1.5 dex over the entire metallicity range shown in Fig. 1, so they are very clearly ruled out, as anticipated by earlier studies of neutrino-driven winds (Woosley et al. 1994; Hoffman et al. 1996, 1997; Roberts et al. 2010). As discussed by Vlasov et al. (2017), magnetic fields sharply reduce the mass ejected by proto-NS winds because of the small fraction of the stellar surface threaded by open magnetic flux lines. The conflict between spherical model yields and observed abundances suggests that most proto-NSs are indeed significantly magnetized. Alternatively, some currently unrecognized neutrino transport physics could alter the ratio of electron and anti-electron neutrino fluxes in the early cooling epoch of the proto-NS wind ( $t \lesssim 2$  s), changing the predicted nucleosynthesis by altering the electron fraction along a given thermodynamic trajectory of the expanding matter.

In Fig. 1, the predicted flat trend of  $[\text{Y}/\text{Fe}]$  without proto-NS winds (red dashed curve) at  $[\text{Fe}/\text{H}] \lesssim -2.0$  is due to the chemical enrichment of Y from the winds of massive stars and Fe from core-collapse SNe. At metallicities in the range  $-1.2 \lesssim [\text{Fe}/\text{H}] \lesssim -0.6$ ,  $[\text{Y}/\text{Fe}]$  decreases because of the large amounts of Fe injected in the ISM by Type Ia SNe. At  $[\text{Fe}/\text{H}] \approx -0.6$ ,  $[\text{Y}/\text{Fe}]$  increases because of the large amounts of Y produced by AGB stars per unit time, which is eventually overcome by Type Ia SNe at  $[\text{Fe}/\text{H}]_{\gtrsim 0}$ . A similar explanation is valid for the predicted trends of  $[\text{Sr}/\text{Fe}]$  and  $[\text{Zr}/\text{Fe}]$ , in agreement with discussion of  $[\text{Sr}/\text{Fe}]$  by Johnson & Weinberg (2020). However, without a proto-NS wind contribution, these trends lie below the data by  $\sim 0.3$ –1 dex.

In Fig. 2, we compare the predictions of our reference chemical evolution model for  $[\text{Ba}/\text{Fe}]$  with the observational data. Models with an additional r-process contribution from neutrino-driven winds of massive proto-NSs ( $M_{\text{Ba,r}} = 5 \times 10^{-7} M_{\odot}$  per event) provide excellent agreement with the bulk of the observational data from the GALAH survey (Buder et al. 2018) as well as with Zhao et al. (2016) and Chaplin et al. (2020), all including NLTE effects in their abundance analysis. Without this contribution, the model underpredicts observed abundances at  $[\text{Fe}/\text{H}] \lesssim -1$ .

It has been shown that the p-rich outflows of proto-NSs can be highly effective in the nucleosynthesis of Mo and Ru (Pruet et al.

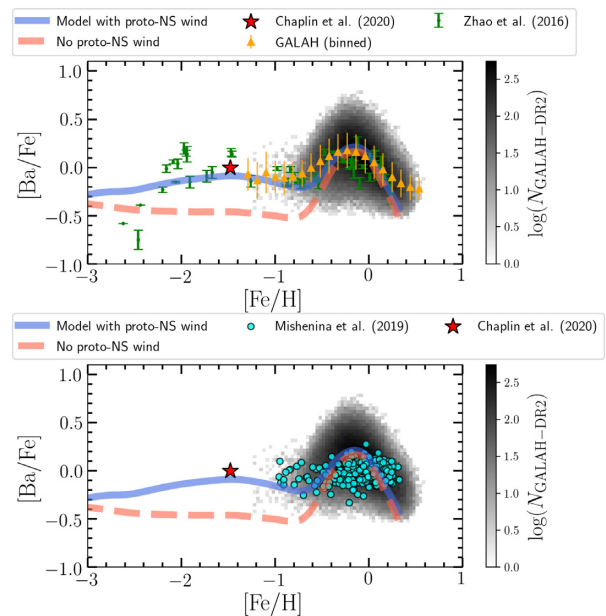


**Figure 2.** The predicted  $[\text{Ba}/\text{Fe}]$ – $[\text{Fe}/\text{H}]$  abundance pattern from our reference chemical evolution model including neutrino-driven winds of massive proto-NSs (blue solid curve) as compared with a model that does not assume proto-NS winds (red dashed curve, like in Fig. 1). For these predictions, we base the Ba yield on the calculations of Wanajo (2013) rather than the much lower Ba yields computed by Vlasov et al. (2017) (see Section 2). The two panels focus on different sets of observational data, which are from Zhao et al. (2016, green error bars), Mishenina et al. (2019, cyan filled circles), and Chaplin et al. (2020, red star symbol). The observational data from GALAH-DR2 (Buder et al. 2018) are shown as in Fig. 1.

2006). In order to test this scenario, in Fig. 3 we compare the predictions of our models for  $[\text{Mo}/\text{Fe}]$  (upper panel) and  $[\text{Ru}/\text{Fe}]$  (lower panel) with a set of observational data (Peterson 2013; Hansen et al. 2014; Spite et al. 2018; Mishenina et al. 2019, 2020). Similarly to what we find for the first- and second-peak s-process elements, our chemical evolution model including proto-NS winds with a production factor  $P = 30$  produces a good match to the bulk of the observational data of  $[\text{Mo}/\text{Fe}]$  and  $[\text{Ru}/\text{Fe}]$  as a function of  $[\text{Fe}/\text{H}]$ , while the model without proto-NS winds falls far short.

### 3.1 The impact of rotating massive stars at low metallicities

The Sukhbold et al. (2016) yields are available only at solar metallicity, and they assume non-rotating massive star progenitors. To address both of these potential shortcomings, we consider the alternative yields of Limongi & Chieffi (2018). Table 1 reports the IMF-averaged  $[\text{X}/\text{Fe}]$  ratios ( $X = \text{Sr}, \text{Y}, \text{Zr}, \text{Ba}$ , and Mo) as predicted when assuming these yields, for different  $[\text{Fe}/\text{H}]$  abundances and rotation velocities. Larger rotation velocity causes an enhancement of the s-process production in massive stars (see also fig. 4 of Johnson & Weinberg 2020); this is due to the so-called rotation-induced mixing, which can bring material from the convective H-burning shell (in particular,  $^{14}\text{N}$  nuclei produced in the CNO cycle) to the He-burning core, where the reaction  $^{22}\text{Ne}(\alpha, n)^{25}\text{Mg}$  takes place (the main source of free neutrons in massive stars). When the  $^{14}\text{N}$  nuclei reach the He-core, they can capture two  $\alpha$ -particles to produce  $^{22}\text{Ne}$ , eventually giving rise to more s-process events. This physical mechanism, which enhances the s-process nucleosynthesis in massive stars, was originally proposed by Frischknecht et al. (2012) to explain the s-

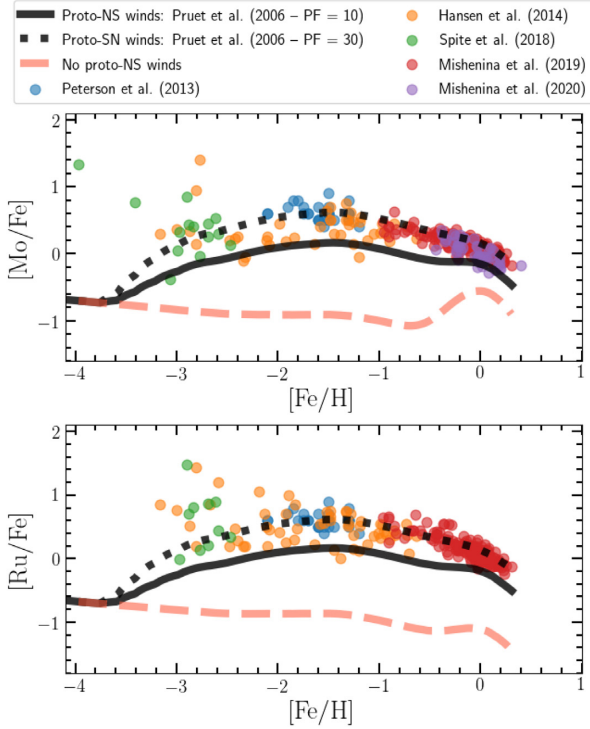


**Figure 3.** Predictions for  $[\text{Mo}/\text{Fe}]$ – $[\text{Fe}/\text{H}]$  (upper panel) and  $[\text{Ru}/\text{Fe}]$ – $[\text{Fe}/\text{H}]$  (lower panel). The black curve corresponds to the models with p-rich outflows from proto-NSs (Pruet et al. 2006), by assuming a production factor (PF) of 10 (black solid curve) and 30 (black dashed curve). The model without the contribution of proto-NS winds is the red dashed line, like in Fig. 1. The observational data are from Peterson (2013, blue filled circles), Hansen, Andersen & Christlieb (2014, orange filled circles), Spite et al. (2018, green filled circles), Mishenina et al. (2019, red filled circles), Mishenina et al. (2020, violet filled circles).

process nucleosynthesis at very low-metallicity (see also Cescutti et al. 2013).

The rotation velocity of massive stars is highly uncertain. One benchmark study is that of Ramírez-Agudelo et al. (2013), who found that the distribution of the projected rotation velocities in a sample of massive stars in the Tarantula Nebula has a peak at  $\sim 80 \text{ km s}^{-1}$ , with the 80th percentile being at  $\approx 300 \text{ km s}^{-1}$ . Therefore, in the context of the stellar models of Limongi & Chieffi (2018), a value of  $v_{\text{rot}} \approx 300 \text{ km s}^{-1}$  should be considered as an approximate upper limit from an observational point of view, with the majority of the stars likely rotating with velocities in the range  $0 < v_{\text{rot}} < 150 \text{ km s}^{-1}$ . However, typical rotation speeds could be different at very low metallicities.

In Fig. 4, we show the predictions of chemical evolution models assuming the stellar nucleosynthesis yields of Limongi & Chieffi (2018) for  $v_{\text{rot}} = 150 \text{ km s}^{-1}$  with and without proto-NS winds (blue solid curve and red dashed curve, respectively, for  $[\text{Ba}/\text{Fe}]$  in the upper panel). We assume yields are constant below  $[\text{Fe}/\text{H}] = -3$ . For comparison, we also show our reference chemical evolution model assuming the stellar yields of Sukhbold et al. (2016) with proto-NS winds ( $P = 5 \text{ ms}$ ; thin dotted line), taking these yields to be metallicity independent. If we do not include proto-NS winds, the predicted  $[\text{Sr}/\text{Fe}]$ ,  $[\text{Ba}/\text{Fe}]$ , and  $[\text{Mo}/\text{Fe}]$  lie well below the Roederer et al. (2014) data at  $-4 \leq [\text{Fe}/\text{H}] \leq -2$ . Conversely, when we include our standard estimate of the r-process contribution from proto-NS winds, we obtain better agreement with the average trend of the observational data at low  $[\text{Fe}/\text{H}]$ . The  $[\text{Sr}/\text{Fe}]$  comparison prefers the

**Table 1.** The IMF-averaged yield of  $[X/\text{Fe}]$  ( $X = \text{Sr}, \text{Y}, \text{Zr}, \text{Ba},$  and  $\text{Mo}$ ) as predicted by the massive star models of Limongi & Chieffi (2018), as a function of  $[\text{Fe}/\text{H}]$  and rotation velocity. The assumed IMF is that of Kroupa et al. (1993). The values in the table are computed by using *gross* stellar nucleosynthetic yields, namely including also the contribution of the ejected material that was present at the stellar birth and remained unprocessed. The IMF-averaged stellar yields are computed by using the code VICE (Johnson & Weinberg 2020). These yields are reported in terms of  $[X/\text{Fe}]$ , where Fe is the IMF-averaged iron yield from massive stars only.

$[\text{Fe}/\text{H}] = -3.0$					
$v_{\text{rot}}/[\text{km s}^{-1}]$	$[\text{Sr}/\text{Fe}]$	$[\text{Y}/\text{Fe}]$	$[\text{Zr}/\text{Fe}]$	$[\text{Ba}/\text{Fe}]$	$[\text{Mo}/\text{Fe}]$
0	−3.55	−3.58	−3.59	−3.59	−3.55
150	−1.97	−2.22	−2.35	−2.85	−2.79
300	1.10	−0.45	−0.24	0.10	−0.21
$[\text{Fe}/\text{H}] = -2.0$					
$v_{\text{rot}}/[\text{km s}^{-1}]$	$[\text{Sr}/\text{Fe}]$	$[\text{Y}/\text{Fe}]$	$[\text{Zr}/\text{Fe}]$	$[\text{Ba}/\text{Fe}]$	$[\text{Mo}/\text{Fe}]$
0	−2.49	−2.54	−2.58	−2.57	−2.56
150	−0.14	−0.25	−0.42	−0.98	−1.00
300	1.41	0.57	0.85	1.10	0.62
$[\text{Fe}/\text{H}] = -1.0$					
$v_{\text{rot}}/[\text{km s}^{-1}]$	$[\text{Sr}/\text{Fe}]$	$[\text{Y}/\text{Fe}]$	$[\text{Zr}/\text{Fe}]$	$[\text{Ba}/\text{Fe}]$	$[\text{Mo}/\text{Fe}]$
0	−1.07	−1.23	−1.38	−1.48	−1.48
150	0.58	0.33	0.01	−0.87	−0.74
300	0.41	1.51	1.81	2.02	1.51
$[\text{Fe}/\text{H}] = 0$					
$v_{\text{rot}}/[\text{km s}^{-1}]$	$[\text{Sr}/\text{Fe}]$	$[\text{Y}/\text{Fe}]$	$[\text{Zr}/\text{Fe}]$	$[\text{Ba}/\text{Fe}]$	$[\text{Mo}/\text{Fe}]$
0	−0.35	−0.44	−0.51	−0.54	−0.54
150	0.37	0.20	−0.05	−0.45	−0.61
300	0.39	0.71	0.51	−0.20	−0.32

higher proto-NS yields of the  $P = 2 \text{ ms}$  models. The chemical evolution model assuming rotating massive stars with  $v_{\text{rot}} = 150 \text{ km s}^{-1}$  and proto-NS winds systematically overestimates  $[\text{Sr}/\text{Fe}]$  at  $[\text{Fe}/\text{H}] \gtrsim -2$ . This disagreement can be alleviated by transitioning to low rotation speeds for  $[\text{Fe}/\text{H}] \gtrsim -2$ , thus moving towards the black dashed curve computed with Sukhbold et al. (2016) stellar yields.

If we assume still higher rotation velocities at low metallicity, then it becomes possible to reproduce the data without the addition of proto-NS winds. Fig. 5 compares the observed chemical abundance ratios of  $[\text{Ba}/\text{Fe}]$  (upper panel),  $[\text{Sr}/\text{Fe}]$  (intermediate panel), and  $[\text{Mo}/\text{Fe}]$  (bottom panel) with the predictions of models assuming the stellar nucleosynthetic yields of Limongi & Chieffi (2018) for  $v_{\text{rot}} = 0, 150,$  and  $300 \text{ km s}^{-1}$ . At least in overall level, the observed  $[\text{Sr}/\text{Fe}]$  and  $[\text{Ba}/\text{Fe}]$  ratios at low metallicities can be explained by models with rotation velocities in the range  $150 < v_{\text{rot}} < 300 \text{ km s}^{-1}$ , without the need of a significant r-process contribution from additional sources. Reproducing the observed  $[\text{Mo}/\text{Fe}]$  requires typical rotation speeds at the top of this range.

## 4 CONCLUSIONS

In this work, we have tested the hypothesis that the observed abundances of first-peak (i.e. Sr, Y, Zr) and second-peak (i.e. Ba) s-process elements, as well as the abundances of Mo and Ru, can be explained by incorporating an additional r-process contribution at low metallicities from neutrino-driven winds from proto-NSs. To this aim, we have developed chemical evolution models for the evolution of the elemental abundances in our Galaxy including proto-NS winds, also investigating the impact of different assumptions for the chemical enrichment of massive stars, which can be important s-

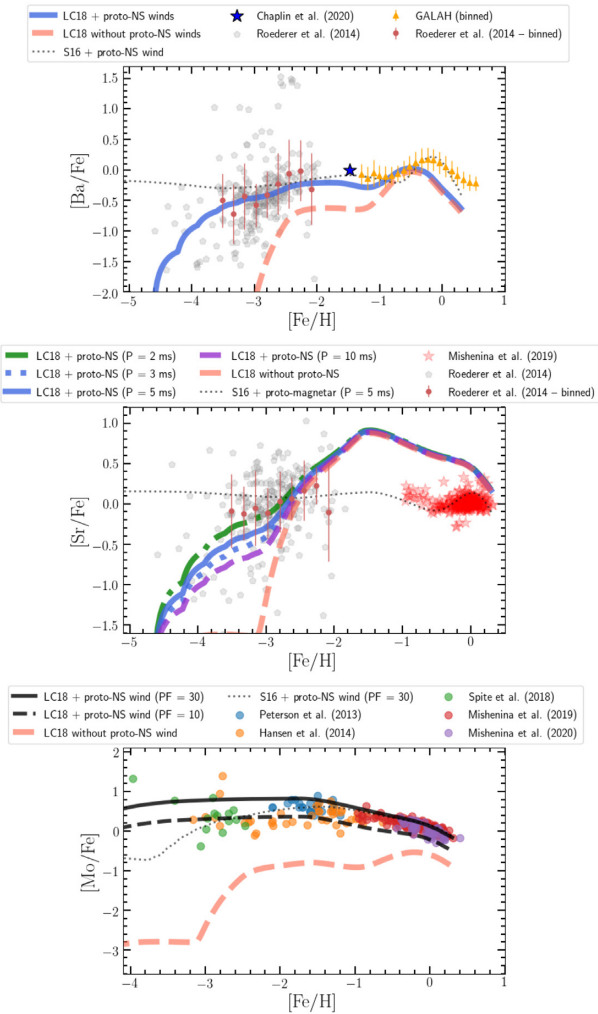


**Figure 4.** Predictions for  $[\text{Ba}/\text{Fe}]$ – $[\text{Fe}/\text{H}]$  (upper panel),  $[\text{Sr}/\text{Fe}]$ – $[\text{Fe}/\text{H}]$  (middle panel), and  $[\text{Mo}/\text{Fe}]$ – $[\text{Fe}/\text{H}]$  (lower panel), focusing on the trend at low metallicities in order to reproduce the observations of Roederer et al. (2014, grey pentagons), which have also been binned in the range  $-3.6 \leq [\text{Fe}/\text{H}] < -2.0$  to determine the mean trend and the dispersion of the data (red point with error bars). We show models assuming the stellar yields of Limongi & Chieffi (2018, LC18; set R) for massive stars ( $v_{\text{rot}} = 150 \text{ km s}^{-1}$ ), the AGB stellar yields of Cristallo et al. (2016), and neutrino-driven winds from proto-NSs (Sr from Vlasov et al. 2017, Ba from Wanajo 2013, and Mo from Pruet et al. 2006). The various curves and the remaining observational data are the same as in Fig. 2. We also show for comparison the prediction of the model with Sukhbold et al. (2016, S16; thin black dotted curve) yields with chemical enrichment from massive stars and proto-NS winds with  $P = 5 \text{ ms}$ . The Sukhbold et al. (2016) yields are computed only for solar metallicity.

process contributors of light neutron-capture elements at low  $[\text{Fe}/\text{H}]$  (Frischknecht et al. 2012; Cescutti et al. 2013).

We base our proto-NS wind yields on the calculations of Vlasov et al. (2017, for Y, Sr, Zr), Wanajo (2013, for Ba), and Pruet et al. (2006, for Mo, Ru). We caution that the Wanajo (2013) Ba yield of  $\approx 5 \times 10^{-7} M_{\odot}$  per event is much higher than the Ba yield predicted by Vlasov et al. (2017), so we regard our Ba predictions as more uncertain (see Section 2 for details). For massive stars, we construct models using the non-rotating models of Sukhbold et al. (2016) computed at  $[\text{Fe}/\text{H}] = 0$ , and alternative models using the yields of Limongi & Chieffi (2018, set R), which are available for different rotation velocities and  $[\text{Fe}/\text{H}]$  abundances. Both Sukhbold et al. (2016)

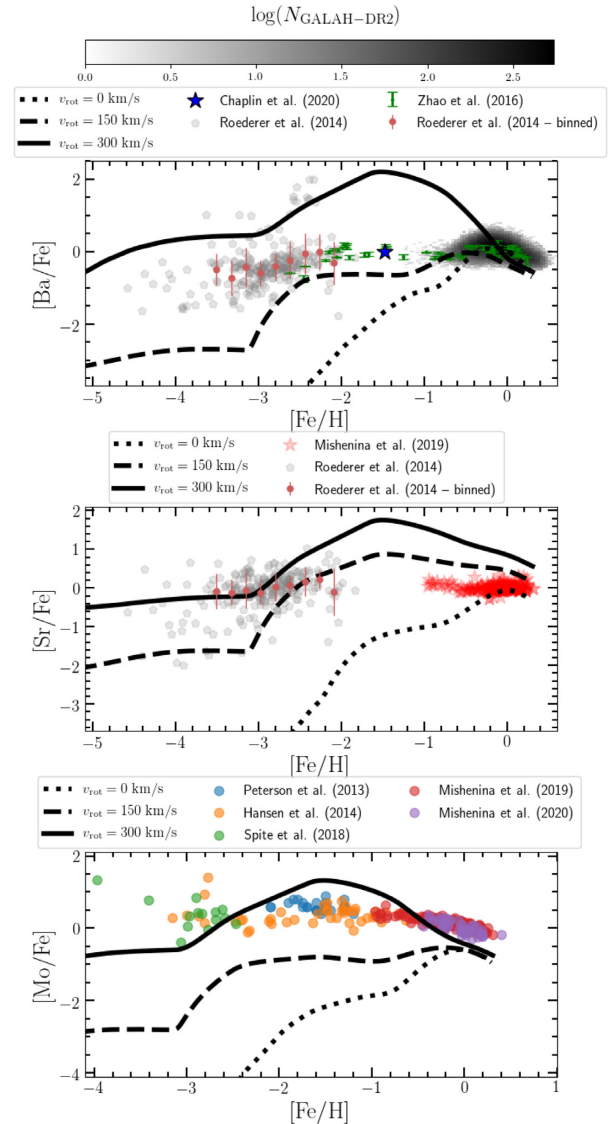


**Figure 5.** Model predictions of  $[\text{Ba}/\text{Fe}]$  (upper panel),  $[\text{Sr}/\text{Fe}]$  (intermediate panel), and  $[\text{Mo}/\text{Fe}]$  (bottom panel) as a function of  $[\text{Fe}/\text{H}]$ , as computed by using the nucleosynthetic stellar yields of Limongi & Chieffi (2018) models. The black dotted curve corresponds to  $v_{\text{rot}} = 0 \text{ km s}^{-1}$ , the black dashed curve to  $v_{\text{rot}} = 150 \text{ km s}^{-1}$ , and the black solid to  $v_{\text{rot}} = 300 \text{ km s}^{-1}$ . The observational data are the same as in Figs 2–4.

and Limongi & Chieffi (2018) massive star models account for failed SNe, but Sukhbold et al. (2016) compute an explosion landscape based on a neutrino-driven central engine, while Limongi & Chieffi (2018) impose a mass threshold for black hole formation at  $25 M_{\odot}$ . Our main conclusion can be summarized as follows.

(i) Adding the predicted proto-NS wind yields to the Sukhbold et al. (2016) massive star yields, and our standard choice of Type Ia SN and AGB yields, leads to good agreement with the observed trends of  $[\text{Y}/\text{Fe}]$ ,  $[\text{Zr}/\text{Fe}]$ ,  $[\text{Sr}/\text{Fe}]$ ,  $[\text{Ba}/\text{Fe}]$ ,  $[\text{Mo}/\text{Fe}]$ , and  $[\text{Ru}/\text{Fe}]$  (see Figs 1–3). The best agreement for Sr, Y, and Zr is obtained for proto-NS rotation periods  $P \sim 2$ – $5 \text{ ms}$ , while models with  $P \sim 10 \text{ ms}$  (which are effectively in the non-rotating limit for our purposes) underpredict the observed  $[\text{Sr}/\text{Fe}]$ . For Mo and Ru, production factors of 10–30 (see equation 1) are required, similar to the proto-NS wind predictions of Pruet et al. (2006). Without proto-NS winds,

the models underpredict the observations by 0.3–1 dex for stars with  $[\text{Fe}/\text{H}] \lesssim -0.5$ , though for Y, Sr, and Ba the AGB contribution leads to acceptable agreement near solar metallicity.

(ii) Because the Sukhbold et al. (2016) yields assume non-rotating, solar metallicity progenitors, we have also considered the alternative yield sets of Limongi & Chieffi (2018) for  $[\text{Fe}/\text{H}] = -3, -2, -1, 0$  and progenitor rotation velocities of  $v_{\text{rot}} = 0, 150, \text{ and } 300 \text{ km s}^{-1}$ . For  $v_{\text{rot}} = 150 \text{ km s}^{-1}$ , we find reasonable agreement with observed  $[\text{Ba}/\text{Fe}]$  and  $[\text{Sr}/\text{Fe}]$  trends for  $-4 < [\text{Fe}/\text{H}] < -2$  with the addition of proto-NS wind yields with  $P = 2\text{--}5 \text{ ms}$  (see Fig. 4). Without proto-NS winds, these models severely underpredict the observed Ba and Sr abundances at  $[\text{Fe}/\text{H}] < -2$ .

(iii) In the range  $-1 \lesssim [\text{Fe}/\text{H}] \lesssim -0.5$ , models with the Limongi & Chieffi (2018)  $v_{\text{rot}} = 150 \text{ km s}^{-1}$  overpredict the observed  $[\text{Sr}/\text{Fe}]$ , even without proto-NS winds (see Fig. 4). This conflict suggests that rotation velocities of massive stars must be lower than  $150 \text{ km s}^{-1}$  at these metallicities.

(iv) The predicted s-process yields of low-metallicity massive stars are sensitive to rotation, increasing by one to three orders of magnitude for  $v_{\text{rot}} = 300 \text{ km s}^{-1}$  versus  $v_{\text{rot}} = 150 \text{ km s}^{-1}$  (see Table 1). Even without proto-NS winds, models with yields intermediate between these two cases could reproduce the observed levels of Ba and Sr at  $[\text{Fe}/\text{H}] < -2$  (see Fig. 5). A model with  $v_{\text{rot}} = 300 \text{ km s}^{-1}$  yields could reproduce the observed levels of Mo, though not the detailed trend. The observations of Ramírez-Agudelo et al. (2013) in the Tarantula nebula favour typical rotation velocities  $< 150 \text{ km s}^{-1}$ , but higher rotation might be possible at low metallicity because of reduced mass-loss and associated angular momentum loss. Very high rotation velocities are disfavoured in some recent chemical evolution models such as those of Prantzos et al. (2018, 2020) and Kobayashi et al. (2020).

(v) Models that adopt the Vlasov et al. (2017) yields for spherical winds from non-rotating, unmagnetized proto-NS are strongly ruled out, overpredicting the observed Sr, Y, and Zr abundances by 1–1.5 dex, in agreement with previous studies (Woosley et al. 1994; Hoffman et al. 1996, 1997; Roberts et al. 2010).

In summary, the winds from proto-NS with rotation periods  $P \sim 2\text{--}5 \text{ ms}$  offer a natural explanation for the observed abundances of Sr, Y, Zr, Mo, Ru, and potentially Ba in MW stars with  $[\text{Fe}/\text{H}] < -0.5$ , where models without this contribution fall short by 0.3–1 dex or even more. Models with rapidly rotating massive stars might be able to reproduce the observed trends without the addition of proto-NS winds, but they would require a finely tuned dependence of rotation velocity on metallicity to satisfy a variety of observational constraints.

The  $P \sim 10 \text{ ms}$  models investigated here can be viewed as a near lower limit to the neutrino-driven wind contribution in the Vlasov et al. (2017) models, as they have strong magnetic fields but minimal rotation, and they are already close to producing the observed levels of Sr, Y, and Zr. Further reducing the predicted yields of these elements would require changing the electron fraction evolution in the cooling proto-NS models, by changing the ratio of the electron and anti-electron neutrino fluxes in the first moments after successful SN explosion.

## ACKNOWLEDGEMENTS

We thank the referee, Friedrich-Karl Thielemann, for many precious and thought-provoking comments and suggestions, which improved the clarity and quality of our work. We thank Tuguldur Sukhbold for providing the set of stellar yields assumed in our chemical evolution

models. We thank Anna Porredon and Sten Hasselquist for useful remarks. This work was supported by NSF grant AST-1909841. FV acknowledges the support of a Fellowship from the Center for Cosmology and AstroParticle Physics at the Ohio State University. TAT was supported in part by NASA grant #80NSSC20K0531. DHW acknowledges support of the Hendricks Foundation at the Institute for Advanced Study.

## DATA AVAILABILITY

The data underlying this article will be shared on reasonable request to the corresponding author.

## REFERENCES

- Adams S. M., Kochanek C. S., Gerke J. R., Stanek K. Z., 2017, *MNRAS*, 469, 1445
- Andrews B. H., Weinberg D. H., Schönrich R., Johnson J. A., 2017, *ApJ*, 835, 224
- Argast D., Samland M., Thielemann F.-K., Qian Y.-Z., 2004, *A&A*, 416, 997
- Asplund M., Grevesse N., Sauval A. J., Scott P., 2009, *ARA&A*, 47, 481
- Basinger C. M., Kochanek C. S., Adams S. M., Dai X., Stanek K. Z., 2021, *MNRAS*, 508, 1156
- Bell E. F., McIntosh D. H., Katz N., Weinberg M. D., 2003, *ApJS*, 149, 289
- Beniamini P., Hotokezaka K., van der Horst A., Kouveliotou C., 2019, *MNRAS*, 487, 1426
- Bollig R., Yadav N., Kresse D., Janka H.-T., Müller B., Heger A., 2021, *ApJ*, 915, 28
- Buder S. et al., 2018, *MNRAS*, 478, 4513
- Burbidge E. M., Burbidge G. R., Fowler W. A., Hoyle F., 1957, *Rev. Mod. Phys.*, 29, 547
- Burrows A., Dessart L., Livne E., Ott C. D., Murphy J., 2007, *ApJ*, 664, 416
- Busso M., Gallino R., Lambert D. L., Travaglio C., Smith V. V., 2001, *ApJ*, 557, 802
- Cameron A. G. W., 1957, *PASP*, 69, 201
- Cardall C. Y., Fuller G. M., 1997, *ApJ*, 486, L111
- Cescutti G., 2008, *A&A*, 481, 691
- Cescutti G., Chiappini C., 2014, *A&A*, 565, A51
- Cescutti G., François P., Matteucci F., Cayrel R., Spite M., 2006, *A&A*, 448, 557
- Cescutti G., Chiappini C., Hirschi R., Meynet G., Frischknecht U., 2013, *A&A*, 553, A51
- Cescutti G., Romano D., Matteucci F., Chiappini C., Hirschi R., 2015, *A&A*, 577, A139
- Chaplin W. J. et al., 2020, *Nat. Astron.*, 4, 382
- Clayton D. D., 1983, *Principles of Stellar Evolution and Nucleosynthesis*, University of Chicago Press
- Cristallo S., Straniero O., Lederer M. T., Aringer B., 2007, *ApJ*, 667, 489
- Cristallo S., Straniero O., Gallino R., Piersanti L., Domínguez I., Lederer M. T., 2009, *ApJ*, 696, 797
- Cristallo S. et al., 2011, *ApJS*, 197, 17
- Cristallo S., Abia C., Straniero O., Piersanti L., 2015a, *ApJ*, 801, 53
- Cristallo S., Straniero O., Piersanti L., Gobrecht D., 2015b, *ApJS*, 219, 40
- Cristallo S., Karinkuzhi D., Goswami A., Piersanti L., Gobrecht D., 2016, *ApJ*, 833, 181
- Curtis S., Ebinger K., Fröhlich C., Hempel M., Perego A., Liebendörfer M., Thielemann F.-K., 2019, *ApJ*, 870, 2
- Ebinger K., Curtis S., Ghosh S., Fröhlich C., Hempel M., Perego A., Liebendörfer M., Thielemann F.-K., 2020, *ApJ*, 888, 91
- Ertl T., Janka H.-T., Woosley S. E., Sukhbold T., Ugliano M., 2016, *ApJ*, 818, 124
- Faucher-Giguère C.-A., Kaspi V. M., 2006, *ApJ*, 643, 332
- Frebel A., 2010, *AN*, 331, 474
- Freiburghaus C., Rosswog S., Thielemann F.-K., 1999, *ApJ*, 525, L121
- Frischknecht U., Hirschi R., Thielemann F.-K., 2012, *A&A*, 538, L2



- Fröhlich C., Hauser P., Liebendörfer M., Martnez-Pinedo G., Bravo E., Hix W. R., Zinner N. T., Thielemann F.-K., 2005, *Nucl. Phys. A*, 758, 27
- Fröhlich C., Martínez-Pinedo G., Liebendörfer M., Thielemann F.-K., Bravo E., Hix W. R., Langanke K., Zinner N. T., 2006, *Phys. Rev. Lett.*, 96, 142502
- Gallino R., Arlandini C., Busso M., Lugaro M., Travaglio C., Straniero O., Chieffi A., Limongi M., 1998, *ApJ*, 497, 388
- Gerke J. R., Kochanek C. S., Stanek K. Z., 2015, *MNRAS*, 450, 3289
- Goriely S., Bauswein A., Janka H.-T., 2011, *ApJ*, 738, L32
- Halevi G., Mösta P., 2018, *MNRAS*, 477, 2366
- Hansen C. J., Bergemann M., Cescutti G., François P., Arcones A., Karakas A. I., Lind K., Chiappini C., 2013, *A&A*, 551, A57
- Hansen C. J., Andersen A. C., Christlieb N., 2014, *A&A*, 568, A47
- Hoffman R. D., Woosley S. E., Fuller G. M., Meyer B. S., 1996, *ApJ*, 460, 478
- Hoffman R. D., Woosley S. E., Qian Y.-Z., 1997, *ApJ*, 482, 951
- Hollowell D., Iben I., 1989, *ApJ*, 340, 966
- Iben I., Renzini A., 1982, *ApJ*, 263, L23
- Iwamoto K., Brachwitz F., Nomoto K., Kishimoto N., Umeda H., Hix W. R., Thielemann F.-K., 1999, *ApJS*, 125, 439
- Johnson J. W., Weinberg D. H., 2020, *MNRAS*, 498, 1364
- Karakas A., Lattanzio J. C., 2007, *Publ. Astron. Soc. Aust.*, 24, 103
- Karakas A. I., Lugaro M., 2016, *ApJ*, 825, 26
- Kobayashi C., 2004, *MNRAS*, 347, 740
- Kobayashi C., Karakas A. I., Lugaro M., 2020, *ApJ*, 900, 179
- Kroupa P., 2001, *MNRAS*, 322, 231
- Kroupa P., Tout C. A., Gilmore G., 1993, *MNRAS*, 262, 545
- Lattimer J. M., Mackie F., Ravenhall D. G., Schramm D. N., 1977, *ApJ*, 213, 225
- Limongi M., Chieffi A., 2018, *ApJS*, 237, 13
- Magrini L. et al., 2018, *A&A*, 618, A102
- Maoz D., Mannucci F., 2012, *Publ. Astron. Soc. Aust.*, 29, 447
- Maoz D., Mannucci F., Nelemans G., 2014, *ARA&A*, 52, 107
- Matteucci F., Romano D., Arcones A., Korobkin O., Rosswog S., 2014, *MNRAS*, 438, 2177
- Metzger B. D., Thompson T. A., Quataert E., 2007, *ApJ*, 659, 561
- Metzger B. D., Thompson T. A., Quataert E., 2008, *ApJ*, 676, 1130
- Minchev I., Chiappini C., Martig M., 2013, *A&A*, 558, A9
- Mishenina T., Pignatari M., Gorbaneva T., Bisterzo S., Travaglio C., Thielemann F.-K., Soubiran C., 2019, *MNRAS*, 484, 3846
- Mishenina T., Shereta E., Pignatari M., Carraro G., Gorbaneva T., Soubiran C., 2020, *J. Phys.*, 24, 3
- Mösta P. et al., 2014, *ApJ*, 785, L29
- Mösta P., Ott C. D., Radice D., Roberts L. F., Schnetter E., Haas R., 2015, *Nature*, 528, 376
- Mösta P., Roberts L. F., Halevi G., Ott C. D., Lippuner J., Haas R., Schnetter E., 2018, *ApJ*, 864, 171
- Nidever D. L. et al., 2014, *ApJ*, 796, 38
- Nishimura N., Takiwaki T., Thielemann F.-K., 2015, *ApJ*, 810, 109
- Nishimura N., Sawai H., Takiwaki T., Yamada S., Thielemann F.-K., 2017, *ApJ*, 836, L21
- Otsuki K., Tagoshi H., Kajino T., Wanajo S.-y., 2000, *ApJ*, 533, 424
- Pejcha O., Thompson T. A., 2015, *ApJ*, 801, 90
- Peterson R. C., 2013, *ApJ*, 768, L13
- Piersanti L., Cristallo S., Straniero O., 2013, *ApJ*, 774, 98
- Prantzos N., Abia C., Limongi M., Chieffi A., Cristallo S., 2018, *MNRAS*, 476, 3432
- Prantzos N., Abia C., Cristallo S., Limongi M., Chieffi A., 2020, *MNRAS*, 491, 1832
- Pruet J., Thompson T. A., Hoffman R. D., 2004, *ApJ*, 606, 1006
- Pruet J., Woosley S. E., Buras R., Janka H.-T., Hoffman R. D., 2005, *ApJ*, 623, 325
- Pruet J., Hoffman R. D., Woosley S. E., Janka H.-T., Buras R., 2006, *ApJ*, 644, 1028
- Qian Y.-Z., Woosley S. E., 1996, *ApJ*, 471, 331
- Ramírez-Agudelo O. H. et al., 2013, *A&A*, 560, A29
- Reichert M., Obergaulinger M., Eichler M., Aloy M. Á., Arcones A., 2021, *MNRAS*, 501, 5733
- Roberts L. F., Woosley S. E., Hoffman R. D., 2010, *ApJ*, 722, 954
- Roederer I. U. et al., 2014, *ApJ*, 791, 32
- Rolfs C. E., Rodney W. S., 1988, *Cauldrons in the Cosmos*, Chicago University Press
- Rosswog S., 2013, *Phil. Trans. R. Soc. A*, 371, 20120272
- Siegel D. M., Barnes J., Metzger B. D., 2019, *Nature*, 569, 241
- Smart S. J., 2009, *ARA&A*, 47, 63
- Spite F., Spite M., Barbuy B., Bonifacio P., Caffau E., François P., 2018, *A&A*, 611, A30
- Spitoni E., Romano D., Matteucci F., Ciotti L., 2015, *ApJ*, 802, 129
- Straniero O., Gallino R., Busso M., Chieffi A., Raiteri C. M., Limongi M., Salari M., 1995, *ApJ*, 440, L85
- Straniero O., Gallino R., Cristallo S., 2006, *Nucl. Phys. A*, 777, 311
- Straniero O., Cristallo S., Gallino R., 2009, *Publ. Astron. Soc. Aust.*, 26, 133
- Straniero O., Cristallo S., Piersanti L., 2014, *ApJ*, 785, 77
- Sukhbold T., Adams S., 2020, *MNRAS*, 492, 2578
- Sukhbold T., Thompson T. A., 2017, *MNRAS*, 472, 224
- Sukhbold T., Ertl T., Woosley S. E., Brown J. M., Janka H.-T., 2016, *ApJ*, 821, 38
- Takahashi K., Witti J., Janka H.-T., 1994, *A&A*, 286, 857
- Thompson T. A., 2003, *ApJ*, 585, L33
- Thompson T. A., ud-Doula A., 2018, *MNRAS*, 476, 5502
- Thompson T. A., Burrows A., Meyer B. S., 2001, *ApJ*, 562, 887
- Thompson T. A., Chang P., Quataert E., 2004, *ApJ*, 611, 380
- Travaglio C., Gallino R., Arnone E., Cowan J., Jordan F., Sneden C., 2004, *ApJ*, 601, 864
- Ugolino M., Janka H.-T., Marek A., Arcones A., 2012, *ApJ*, 757, 69
- Ulrich R. K., 1973, in Schramm D. N., Arnett D. W., eds, *Explosive Nucleosynthesis*, University of Texas Press, Austin, TX, p. 139
- Vincenzo F., Matteucci F., Recchi S., Calura F., McWilliam A., Lanfranchi G. A., 2015, *MNRAS*, 449, 1327
- Vincenzo F., Matteucci F., Spitoni E., 2017, *MNRAS*, 466, 2939
- Vlasov A. D., Metzger B. D., Thompson T. A., 2014, *MNRAS*, 444, 3537
- Vlasov A. D., Metzger B. D., Lippuner J., Roberts L. F., Thompson T. A., 2017, *MNRAS*, 468, 1522
- Wanajo S., 2013, *ApJ*, 770, L22
- Wanajo S., Janka H.-T., 2012, *ApJ*, 746, 180
- Wanajo S., Nomoto K., Janka H.-T., Kitaura F. S., Müller B., 2009, *ApJ*, 695, 208
- Weinberg D. H., Andrews B. H., Freudenburg J., 2017, *ApJ*, 837, 183
- Winteler C., Käppeli R., Perego A., Arcones A., Vasset N., Nishimura N., Liebendörfer M., Thielemann F.-K., 2012, *ApJ*, 750, L22
- Woosley S. E., Wilson J. R., Mathews G. J., Hoffman R. D., Meyer B. S., 1994, *ApJ*, 433, 229
- Zhao G. et al., 2016, *ApJ*, 833, 225

This paper has been typeset from a  $\text{\LaTeX}$  file prepared by the author.